On-ground Aircraft Modeling for Advanced Braking Control System Design

Amath Waly Ndiaye, Mario Cassaro, Clément Combier, Jean-Marc Biannic, Clément Roos

On-ground Aircraft Modeling for Advanced Braking Control System Design

Amath Waly Ndiaye[1,2], Mario Cassaro[2], Clément Combier[1], Jean-Marc Biannic[2], Clément Roos[2]

***Abstract*— An original simplified 6-DOF on-ground aircraft model is developed, with the intent of providing an efficient means for novel braking control law synthesis. The proposed modeling approach consists of including the entire set of contributing dynamics, during aircraft high-speed braking, scaling the level of complexity and fidelity in function of the dominance of each physical phenomenon described. To this end, simplistic aerodynamic and propulsive models are coupled with a very detailed landing gear mathematical description, including shock-absorber, wheel-ground interaction and tire dynamics. Different modeling techniques are employed, such as analytical, parametric or tabulated models, depending on the subsystem nature and the related available data. The complete aircraft on-ground model is finally validated against a fully nonlinear multi-body simulator available at Safran Landing Systems. The proposed approach demonstrates high fidelity behavior, being capable of capturing critical phenomena such as load transfer between landing gear struts and wheel longitudinal-vertical dynamic coupling, while remaining simple and suitable for a control design purpose. Pertinent results are provided and discussed at the end of the paper.**

I. INTRODUCTION

Despite the recent considerable enhancement of flight control and automation, aircraft on-ground control remains today a major issue which shows some room for improvement. Aircraft runway excursions occurring during landing, i.e. overruns and veer-offs, [1], [2], represent a growing percentage of the overall aircraft accident records, [3], [4]. In addition, a real need of enhancing functionalities on-ground has recently arisen. Recent advances as runway center-line keeper [5], Brake-To-Vacate (BTV) and the automatic taxi guidance [6] functions, are already under development if not already in service [7]. In this context, accurate simulation models for novel control architecture design and validation are relevant for safety, runway management and operability improvement. To this purpose, the long lasting problem of an accurate but simple, amenable for control synthesis, aircraft on-ground model remains topical. Two aircraft on-ground modeling alternatives are mainly employed in present days: 6 degrees-of-freedom (DOF) multi-body models [8], [9], [10]; and 3-DOF reduced order models (ROM), usually obtained by decoupling planar and vertical dynamics [11], [12], [5]. The first solutions generally include detailed description of all mechanical links, physical constraints and nonlinearities (*i.e.* magnitude and rate limiters, dead zones, hysteresis, etc.), resulting in high fidelity and computationally expensive co-simulation environments. Such models are mostly exploited for a validation purpose, but they lead to simplistic control laws design due to their poor tractability by control theory. On the contrary, a 3-DOF ROM, despite its ease of manipulation for control oriented formulation, might loose accuracy in the description of some critical phenomena when advanced braking system design is concerned. As an example, varying tire-road interaction and landing gear structural dynamics are usually neglected, implying the disappearance of gear walk and shimmy phenomena [9]. In addition, most control-design oriented on-ground models found in the literature, unlike the quarter car models in automotive, disregard wheel inherent dynamics or fail to capture normal load transfer, while both are crucial for anti-skid control design purposes [13]. The proposed research aims to derive and implement a complete but simplified 6-DOF on-ground aircraft model, simultaneously capable of capturing the largest possible set of phenomena involved during high-speed braking, and amenable for robust and nonlinear control synthesis. The approach relies on modeling reliably the tire/ground friction and the vertical reaction variations induced by braking. The former is modeled through a parametric empirical formulation of the longitudinal friction, able to fit a wide range of experimental data, coupled with a simplified lateral friction formulation valid for small angles, which is a verified assumption during roll-out phase. Accurate descriptions of the oleo-pneumatic shock-absorbers and the aircraft overall dynamics allow to model precisely the vertical forces and load transfers induced, while simplified aerodynamic and propulsion systems complete the model.

The proposed modeling is validated against a high-fidelity multi-body simulator available at Safran Landing Systems, through a selection of meaningful scenarii. The obtained results confirm the quality of the final model and successfully validate the accuracy of the proposed approach for control synthesis purposes. The paper is organized as follows: the aircraft model is first presented in section II and the validation is then realized in section III. The main contribution resides in the ground interaction model which describes accurately wheel dynamics and the associated contact patch friction forces, as well as the aircraft vertical loads, captured through landing gear vertical dynamics. The proposed on-ground aircraft model remains largely tractable from a control perspective and should allow the design and preliminary validation of more reliable and better performing antiskid braking systems, while still addressing lateral control issues.

[1]Safran Landing Systems, 7 rue Général Valérie André, 78140 Vélizy-Villacoublay, France amath-waly.ndiaye; clement.combier @safrangroup.com

[2]ONERA The French Aerospace Lab, 2 avenue Edouard Belin, 31400 Toulouse, France. mario.cassaro; jean-marc.biannic; clement.roos @onera.fr

II. AIRCRAFT ON-GROUND MODELING

When it comes to on-ground simulation, providing a reliable control oriented aircraft model is troublesome, notably due to tire and shock-absorber nonlinear behaviors [9]. Most of the models available in the literature are essentially focused on lateral control design. Indeed, either cross-coupling behavior induced by tire combined slip is not captured by such models, as in [14], [11] and [12], or, when coupling is considered, the wheel rotational motion is often not described, leading to relatively simple longitudinal forces modeling. This is the case in [15] and [5], where the grip moment is approximated by the braking torque. Besides inaccurate friction and slip dynamics representations, tire and strut vertical dynamics are often not modeled, while they constitute the key parameters in ground phase simulations, as recalled in [16]. Indeed, these variables are essential to predict tire skid, hence the need for an aircraft model incorporating more rigorously the ground interaction effects. In this paper, an emphasis is put on depicting precisely the wheel inherent dynamics and the landing gear load variations, strengthening the accuracy of the depending tire/ground friction forces derived. The latter are modeled via empirical parameterized friction functions handling combined slip conditions. Hence, the proposed model bridges the gap between the lateral control oriented contributions cited above and an exclusively antiskid design oriented modeling, allowing to address the complete control problem of a decelerating aircraft on-ground, in a single environment. The central contribution of this paper can be seen as a continuation of [15], [5]'s work where the derived model does not account for aircraft vertical and wheel slip dynamics. The tire/ground friction forces herein proposed are also more realistic since the depletion occurring for large slip values or combined condition is factored in. Thus, the ground interaction model is enhanced, leading to a valid model regarding braking control laws design and validation. Simple equations are added to the basic aerodynamics and propulsive models to account for 6-DOF motion.

A. Main Assumptions and General Equations

The present model represents an aircraft on the ground during the typical operating condition consisting of braking while keeping runway center line alignment, a situation arising from a landing touchdown or an aborted take-off. In order to derive a sufficiently accurate but still tractable model for braking control design, the following assumptions are considered valid for the motion of the aircraft on-ground, without any significant loss of generality:

$(A1)$ Perfectly horizontal runway.

$(A2)$ Perfectly vertical landing gear structure, *i.e.* strut camber, rake and splay angles are null.

$(A3)$ Perfectly horizontal thrust vector, *i.e.* engines' canting angle is null.

$(A4)$ Equivalent single wheel landing gear.

$(A5)$ Small angles approximation, including nose wheel steering angle θ_{NW}, wheel sideslip angles β_{ti} (where subscript i may be NW, MGR and MGL for nose wheel, main gear right and main gear left respectively), aircraft roll and pitch angles.

$(A6)$ Linearized expressions for the aerodynamic efforts, symmetrical and constant configurations for the ailerons and the elevators, and a negligible wind velocity vector component along $\vec{z}_b$ ($W = [W_x\, W_y\, 0]^T$ in $\mathscr{R}_b$, see Fig. 1) are assumed.

$(A7)$ Rigid body equations of motion.

Assumptions $(A1-A3)$ allow for lightening the mathematical formulation of the external forces and moments, reducing the number of rotation matrices to be taken into account. $(A5)$ allows for removing unnecessary nonlinearities with reference to the operating domain under analysis. $(A4)$ is common practice when neglecting out of the wheel plane dynamics, mostly due to elastic cross-coupling like gear-walk and shimmy. $(A7)$ derives from neglecting structure flexibility, which effects are considered as exogenous perturbations from a control point of view, and so forth not accounted for during control synthesis, but only during robustness analysis.

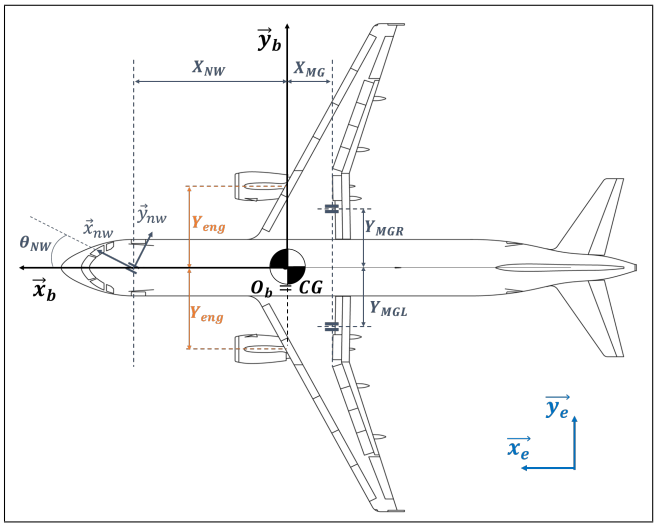

Fig. 1. Aircraft top view, $\mathscr{R}_b$ body reference frame, $\mathscr{R}_{nw}$ nose wheel reference frame, $\mathscr{R}_e$ earth fixed reference frame

Considering the aforementioned assumptions, the general expression of a 6-DOF rigid body aircraft motion in the conventional body reference system $\mathscr{R}_b$, displayed in Fig. 1, reads as follows (see [17]):

$$\begin{aligned}\begin{bmatrix}\dot{u}\\ \dot{v}\\ \dot{w}\end{bmatrix} &= \frac{1}{m}\begin{bmatrix}F_{xeng}+F_{xa}+F_{xt}\\ F_{ya}+F_{yt}\\ mg+F_{za}+F_{zt}\end{bmatrix} - \begin{bmatrix}p\\ q\\ r\end{bmatrix}\wedge\begin{bmatrix}u\\ v\\ w\end{bmatrix}\\ \begin{bmatrix}\dot{p}\\ \dot{q}\\ \dot{r}\end{bmatrix} &= I^{-1}\left(\begin{bmatrix}M_{xa}+M_{xt}\\ M_{yeng}+M_{ya}+M_{yt}\\ M_{zeng}+M_{za}+M_{zt}\end{bmatrix} - \begin{bmatrix}p\\ q\\ r\end{bmatrix}\wedge\left(I.\begin{bmatrix}p\\ q\\ r\end{bmatrix}\right)\right)\end{aligned} \tag{1}$$

where g is the gravity; $\vec{V}_b = [u,v,w]^T$ and $\vec{\Omega}_b = [p,q,r]^T$ denote the center of gravity (CG) linear and angular velocity vectors; m and I represent the aircraft mass and inertia matrix defined at its CG; F_{kj} (resp. M_{kj}) is the total force (resp. moment) along k axis induced by j acting on the aircraft CG.

The subscript j indicates engines thrust (eng), aerodynamic effects (a), gravity (g) or tire/ground interactions (t).

As is clear from (1), the degree of complexity of an aircraft model is strictly related to the chosen formulation for describing the external forces and moments, which is the aim of the next subsections. Fig. 2 depicts the global architecture of the proposed model and highlights the relationships between the different blocks, including the ground interaction model. The latter, fundamental regarding ground simulations and antiskid design, is further detailed in Fig. 8.

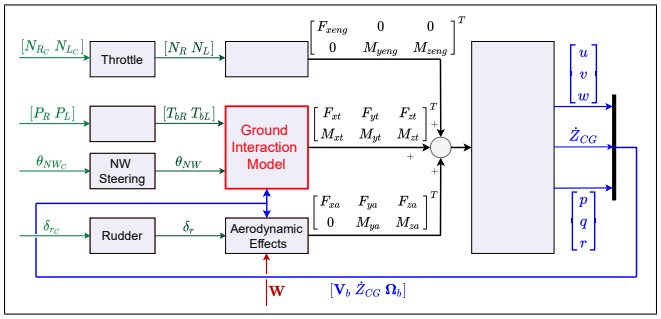

Fig. 2. Aircraft model global architecture

B. Aerodynamic Model

The aerodynamic model used is the same as in [5], [11]. Given the wind velocity vector expressed in $\mathscr{R}_b$, $\vec{W} = [W_x, W_y, 0]^T$, and considering a largely negligible aircraft vertical velocity w, the aerodynamic velocity $\vec{V}_a$ is obtained as :

$$\vec{V}_a = \vec{V}_b - \vec{W} = \begin{pmatrix} v_{ax} \\ v_{ay} \\ 0 \end{pmatrix} |_{\mathscr{R}_b} \tag{2}$$

Thanks to assumption $(A6)$, the forces and moments are computed considering linearized aerodynamic coefficients with a null angle of attack:

$$\begin{aligned} F_{xa} &= q_d\, S\, C_{x0} \\ F_{ya} &= q_d\, S\, (C_{y_\beta}\, \beta + C_{y_r}\, \frac{rc}{v_a} + C_{y_{\delta_r}}\, \delta_r) \\ F_{za} &= q_d\, S\, C_{z0} \\ M_{ya} &= q_d\, S\, C_{m0} \\ M_{za} &= q_d\, S\, c\, (C_{n_\beta}\, \beta + C_{n_r}\, \frac{rc}{v_a} + C_{n_{\delta_r}}\, \delta_r) \end{aligned} \tag{3}$$

where $q_d = \frac{1}{2}\rho v_a^2$ is the dynamic pressure, $v_a = \|\vec{V}_a\|$ is the airspeed while S and c respectively denote the reference surface and the aerodynamic mean chord. The drag, lateral, yaw, lift and pitch stability derivatives are referred to by C_{x0}, C_{y_j}, C_{n_j}, C_{z0} and C_{m0} respectively (j represents either the aerodynamic sideslip angle β, the yaw rate r or the rudder deflection δ_r).

C. Actuators

1) Brakes, Rudder and Engines: First-order actuation dynamics are used to model electrohydraulic brakes, rudder and engines in (4a), (4b) and (4c) respectively. The throttle N_i (resp. rudder deflection δ_r), where i denotes left (L) or right (R), and its rate of variation are bounded according to $N_i \in [N_{IDLE}, N_{MAX}]$ and $\dot{N}_i \in [-L_{reng}, L_{reng}]$ (resp. $|\delta_r| \leq L_{p\delta_r}$ and $|\dot{\delta}_r| \leq L_{r\delta_r}$).

$$\tau_h\, \dot{P}_i + P_i = K_{sv_i}\, I_{sv_i} \tag{4a}$$
$$\tau_{\delta_r}\, \dot{\delta}_r + \delta_r = \delta_{r_c} \tag{4b}$$
$$\tau_N\, \dot{N}_i + N_i = N_{ic} \tag{4c}$$

$(.)_c$ and $\tau_{.}$ represent the reference commanded value and the associated time constant. P, K_{sv} and I_{sv} are the hydraulic pressure, brake gain and servovalve control current respectively. The braking torque T_b and engine thrust F_{xeng} are obtained by:

$$T_{bi} = max(0, K_b\, \Delta P_i) \tag{5a}$$
$$F_{xeng} = -(N_R\, T_{eng_R} + N_L\, T_{eng_L}) \tag{5b}$$

where T_{eng_R} (resp. T_{eng_L}) represents the right (resp. left) engine nominal gain, while K_b is a constant gain and the effective pressure is expressed as $\Delta P = P - P_0$, where P_0 denotes the zero torque pressure required for the pistons to come into contact with the brake discs. The resulting moments of the engines on the aircraft are:

$$\begin{aligned} M_{yeng} &= Z_{eng}\, (N_R\, T_{eng_R} + N_L\, T_{eng_L}) \\ M_{zeng} &= Y_{eng}\, (N_L\, T_{eng_L} - N_R\, T_{eng_R}) \end{aligned} \tag{6}$$

where Z_{eng} and Y_{eng} respectively denote the vertical and lateral position of the engines with respect to the CG, see Fig. 1.

2) Steering System: The steering system actuator dynamics is neglected, and the self-aligning moment $M_{z_{NW}}$ (see Fig. 3) is supposed to be exactly counteracted by the steering torque σ_{steer}:

$$\sigma_{steer} = -M_{z_{NW}} = t_{p_{NW}}\, F_{yt_{NW}} \tag{7}$$

where $t_{p_{NW}}$ is the nose wheel pneumatic trail represented in Fig. 3.

D. Ground Interaction Model

As depicted in Fig. 3, the tire/ground interaction generates longitudinal and lateral friction forces F_{xt_i} and F_{yt_i}, as well as a vertical reaction force F_{zt_i}. The subscript i refers to the nose wheel, main right and left landing gears (respectively NW, MGR and MGL) across the entire paper. Accurate estimation of the ground interaction forces set, $F_{(x,y,z)t_i}$, requires precise modeling of wheel and shock-absorber dynamics, as described in the following subsections.

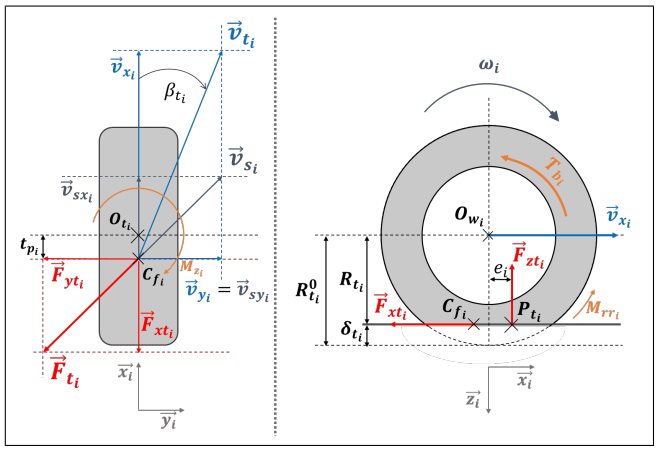

Fig. 3. Tire kinematics: top and side views (C_f (resp. P_t): center of lateral friction (resp. vertical pressure))

1) Vertical Forces: As shown in Fig. 5, a landing gear assembly suspension system can be modeled by a 2-DOF mechanism, comprising a sprung mass - the fuselage, and an unsprung mass - the wheel and its mounted elements. The shock-absorber, subscript *sa*, is modeled as a parallel spring/damper system, with varying parameters k_{sa_i}/b_{sa_i}, while the tire is considered as a simple spring of constant stiffness k_{t_i}.

Since each gear is comprised of two wheels which are subject to exactly the same forces (*A*4), the total ground interaction forces are expressed as:

$$\begin{bmatrix} F_{xt} \\ F_{yt} \\ F_{zt} \end{bmatrix} = 2 \begin{bmatrix} F_{xt_{NW}} + F_{xt_{MGR}} + F_{xt_{MGL}} \\ F_{yt_{NW}} + F_{yt_{MGR}} + F_{yt_{MGL}} \\ F_{zt_{NW}} + F_{zt_{MGR}} + F_{zt_{MGL}} \end{bmatrix} \tag{8}$$

A standard formulation of the vertical loads is:

$$F_{zsa_i} = F_{s_i} + F_{d_i} + F_{sf_i} + F_{bf_i} \tag{9a}$$

$$F_{zt_i} = -k_{t_i}\,\delta_{t_i} \tag{9b}$$

where F_{s_i}, F_{d_i}, F_{sf_i} and F_{bf_i} are the gas spring stiffness, fluid damping, seals and bearings friction forces respectively. δ_{t_i} is the tire compression ($\delta_{t_i} \geq 0$).

The friction forces oppose the motion and contribute to dampen the oscillations ([18]). As computed in [19] the following expressions are assumed for each strut:

$$F_{sf_i} = \mu_{s_i}\, F_{s_i}\, sign(\dot{\delta}_{sa_i}) \tag{10a}$$

$$F_{bf_i} = \mu_{b_i}\, |F_{xt_i}|\, sign(\dot{\delta}_{sa_i}) \tag{10b}$$

where δ_{sa_i} is the shock-absorber stroke ($\dot{\delta}_{sa_i} > 0$ in compression), while μ_{s_i} and μ_{b_i} are the seal and bearing kinetic friction coefficients respectively.

The gas spring force F_{s_i} takes into account the thermal hysteretic effects arising from unequal heat transfers between the gas and its surroundings. As explained in [20], [21], [22], the gas compression/extension is not an ideal adiabatic process, hence the shock-absorber nonlinear spring curve displays an irreversible behavior highlighted in Fig 4. The force during a sufficiently high amplitude compression (blue curve) is higher than during the corresponding extension (red curve). The oscillating regime at constant stiffness k_i (yellow area), which characterizes the transition between both curves, derives from small volume variation hypothesis for a perfect gas [20]. Thus, during a drop test or landing first compression/extension strut cycle, the first amplitude of F_{s_i} is determined by the blue curve from $(0;0)$ to point A, then the shock-absorber undergoes a brief extension of linear force variation (pink dashed line) from A to B, followed by an extension $B-C$ along the red curve f_{rec}. The second compression force variation is partly linear ($C-D$), partly on f_{comp} ($D-E$), while the second rebound allows to reach the point F in the oscillating regime. The remaining variations of F_{s_i} are exclusively linear (relative to the stroke δ_{sa}), of constant stiffness k_i around an equilibrium point along the dashed curve containing point F (oscillating regime). In that respect, the spring force takes the following expression, subscript i being omitted for ease of reading:

$$F_s = \begin{cases} \min\left(f_{comp}(\delta_{sa}),\, f_0 + k\,\delta_0\right) & \text{if } \dot{\delta}_{sa} > 0 \\ \max\left(f_{rec}(\delta_{sa}),\, f_0 + k\,\delta_0\right) & \text{if } \dot{\delta}_{sa} < 0 \end{cases} \tag{11}$$

where f_{comp} and f_{rec} are the stroke dependent compression and recoil forces. f_0 and δ_0 are the shock force and stroke at the start of the switching motion point (recoil to compression and vice-versa). In the previous motion described, the successive values of $(\delta_{0\,comp}, f_{0\,comp})$ represent the coordinates of A and E. The main landing gear spring curves present a slope discontinuity typical of two-stage shock-absorbers as can be noticed in Fig. 4.

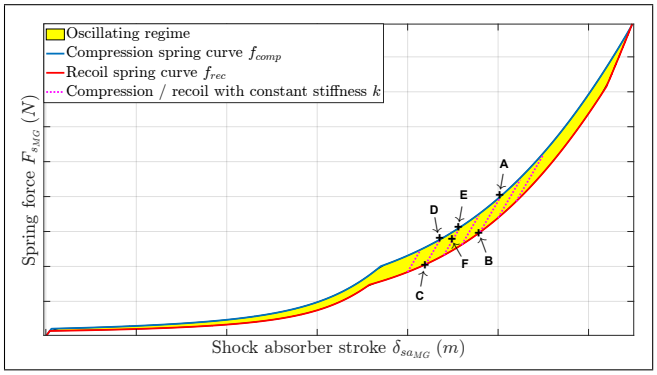

Fig. 4. Spring force model (Safran proprietary data have been deliberately distorted)

The damping force F_{d_i} arises from turbulent energy dissipation during fluid flow through the shock-absorber valves and is proportional to the square of the stroke velocity. However, as explained in [23], for low shock-absorber compression/extension velocities, the progressive opening of shim valves yields a regressive dependence of the pressure drop on fluid flow rate, so that F_{d_i} is proportional to $|\dot{\delta}_{sa_i}|$ to the power $\frac{2}{3}$. Hence, the following model is proposed to cope with such low velocities which typically appear during taxiing and braking maneuvers:

$$F_{d_i} = \begin{cases} b_{sa_i}\dot{\delta}_{sa_i}^2 sign(\dot{\delta}_{sa_i}) & \text{if } |\dot{\delta}_{sa_i}| \geq V_{tr} \\ B_{sa_i}|\dot{\delta}_{sa_i}|^{\frac{2}{3}} sign(\dot{\delta}_{sa_i}) & \text{if } |\dot{\delta}_{sa_i}| < V_{tr} \end{cases} \quad (12)$$

where b_{sa_i}/B_{sa_i} and V_{tr} are respectively the high/low velocity damping coefficients and the stroke transition velocity. Equating both expressions of (12) at $|\dot{\delta}_{sa_i}| = V_{tr}$ results in $B_{sa_i} = b_{sa_i} V_{tr}^{\frac{4}{3}}$. To handle the discontinuity and subsequent numerical issues introduced by the sign function in (10a), (10b) and (12), a smooth hyperbolic tangent function can be used as explained in [24], [25], [26].

δ_{sa_i} and δ_{t_i} are computed by including each component dynamics in the model. In detail, the velocity difference between both attachment points of the shock-absorber gives (13), relating the stroke and tire compression rates of variation $\dot{Z}_{sa_i}$ and $\dot{\delta}_{t_i}$, the aircraft CG height Z_{CG}, and the coordinates X_i and Y_i of the landing gear considered ($i \in \{NW; MGR; MGL\}$). Newton's second law applied to the wheel, of mass m_i, leads to (14).

$$\dot{Z}_{sa_i} = -\dot{\delta}_{sa_i} = \dot{Z}_{CG} + q X_i - p Y_i - \dot{\delta}_{t_i} \quad (13)$$

$$\ddot{R}_{t_i} = -\ddot{\delta}_{t_i} = \frac{F_{zt_i} - \frac{1}{2}F_{zsa_i}}{m_i} - g \quad (14)$$

As is clear from (13) the stroke dynamics is function of the aircraft CG vertical motion and angular rates, together with the tire compression dynamics. The latter, described by (14), is itself function of the wheel mass m_i, as well as tire and shock-absorber vertical loads. The computation of δ_{sa_i} and δ_{t_i} implies the implementation of an internal dynamic loop to resolve the parameters inter-dependency (as later depicted in Fig. 8).

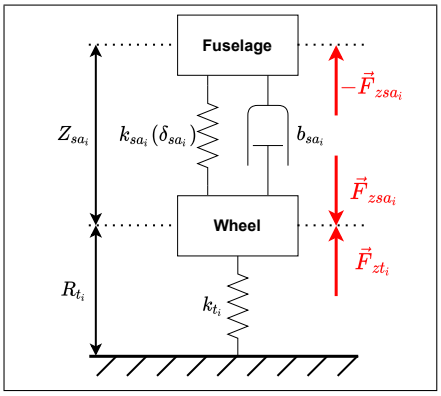

Fig. 5. Single gear model (k_{sa} is either equal to the constant stiffness k or to $\frac{\partial f_{comp.rec}}{\partial \delta_{sa}}$, cf. Fig. 4)

2) Longitudinal and Lateral Friction Forces: As reported in Fig. 3, the projection of the total tire force vector $\vec{F}_{t_i}$ on the ground plane is directed opposite to the slip velocity vector v_{s_i} (coordinates: $v_{sx_i} = v_{x_i} - R_{t_i}\omega_i$, $v_{sy_i} = v_{y_i}$). A general expression of its components F_{xt_i} and F_{yt_i}, can be written as in [27], as a function of the vertical load and the corresponding friction coefficients μ_x and μ_y:

$$F_{xt,yt_i}(\lambda_i, \beta_{t_i}) = -|F_{zt_i}| \cdot \mu_{x,y}(\lambda_i, \beta_{t_i}) \quad (15)$$

where the independent parameters λ_i and β_{t_i} denote the longitudinal slip ratio ($0 \leq \lambda_i \leq 1$) and the lateral sideslip angle respectively, defined as in [28]:

$$\lambda_i = \frac{v_{x_i} - R_{t_i}\omega_i}{v_{x_i}} \quad (16)$$

$$\beta_{t_{MGR,L}} = \frac{v_{y_{MGR,L}}}{v_{x_{MGR,L}}} = \frac{v + r X_{MGR,L}}{u - r Y_{MGR,L}} \quad (17a)$$

$$\beta_{t_{NW}} = \frac{v_{y_{NW}}}{v_{x_{NW}}} - \theta_{NW} = \frac{v + r X_{NW}}{u - r Y_{NW}} - \theta_{NW} \quad (17b)$$

where the geometric parameters, X_i and Y_i, are defined as in Fig.3 and Fig. 1, while the rotational velocity ω_i is derived in (22). The nose wheel steering angle θ_{NW} is supposed to be exactly equal to its commanded value θ_{NW_c} according to (7).

In the perspective of obtaining a simple but accurate model for anti-skid control design, the modeling of tire/ground friction phenomena are of paramount importance. To this end, starting from a specific empirical formulation employed at Safran Landing Systems, an original modification to account for cross coupling effects is proposed in this paper. The friction coefficients expressions considering pure longitudinal and lateral conditions are written as follows, subscript i being omitted for ease of reading:

$$\mu_x(\lambda, \beta_t = 0) = \begin{cases} \frac{2\,\lambda\,\lambda_{opt}\,\mu_m}{\lambda^2 + \lambda_{opt}^2} & \text{if } \lambda < \lambda_{opt} \\ \mu_l + (\mu_m - \mu_l) e^{-\frac{1}{2}\left(\frac{\lambda - \lambda_{opt}}{\sigma}\right)^{\gamma}} & \text{if } \lambda \geq \lambda_{opt} \end{cases} \quad (18)$$

$$\mu_y(\lambda = 0, \beta_t) = k_1 (1 - e^{-k_2|\beta_t|})\, sign(\beta_t) \quad (19)$$

where μ_m and μ_l correspond to the maximum and locked-wheel friction coefficients respectively, while λ_{opt} is the slip ratio value at μ_m, corresponding to the peak of the friction curve in Fig. 6. The values of these parameters along with those of the fitting empirical coefficients γ, σ, k_1 and k_2 can be found in Table I.

The proposed formulation includes the mutual longitudinal-lateral interference by adding another step of computation, which consists of an exponentially decaying cross-coupling term. The two coefficients illustrated in Fig. 6 and Fig. 7 are finally obtained as:

$$\mu_x(\lambda, \beta_t) = (c_1 + c_2 e^{-c_3|\beta_t|})\, \mu_x(\lambda, \beta_t = 0) \quad (20)$$

$$\mu_y(\lambda, \beta_t) = (k_3 + k_4\, e^{-k_5 \lambda})\, \mu_y(\lambda = 0, \beta_t) \quad (21)$$

where $c_{1,2,3}$ and $k_{3,4,5}$ are positive fitting coefficients (see Table I).

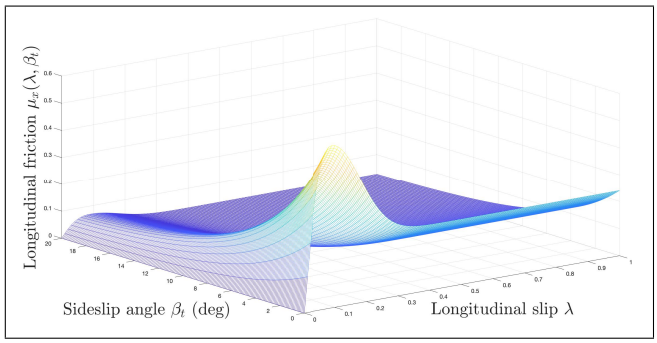

Fig. 6. Longitudinal friction $\mu_x(\lambda,\beta_t)$ (dry runway)

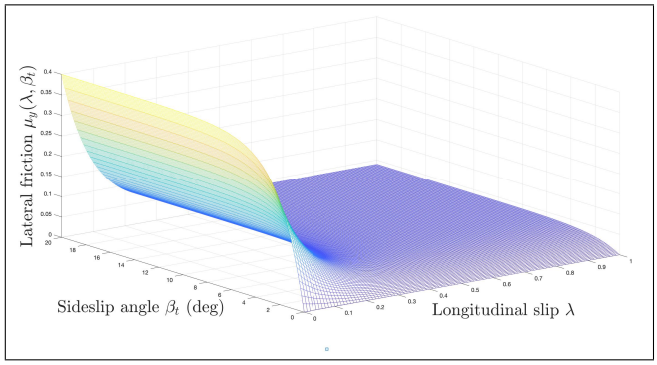

Fig. 7. Lateral friction $\mu_y(\lambda,\beta_t)$ (dry runway)

3) Wheel Rotational Dynamics: The standard equation of motion describing the rotation of the wheel is given by:

$$J_i\,\dot{\omega}_i = T_{b_i} + M_{rr_i} - F_{xt_i}\,R_{t_i} \tag{22}$$

where J_i is the wheel inertia. M_{rr_i} is the wheel rolling resistance moment ($M_{rr_i} = e_i\,F_{zt_i}$, see Fig. 3), while T_{b_i} is the applied braking torque, given by (5a). It should be recalled that the nose wheels are not braked ($T_{b_{NW}} = 0$).

It should be noticed that unlike [5], there is no rolling resistance term F_r in (22) as this force is captured through the impact of M_{rr} which tends to decelerate the wheel even when no braking torque is applied. The resulting wheel slip increase (see (16) and (20)) generates a non zero value of the longitudinal force $F_{xt}(\lambda,\beta_t)$ at free rolling, accounting for this rolling resistance force. Another aspect not considered is tire load sensitivity, namely the impaired friction for increasing vertical load values. This assumption that friction coefficients and vertical load are independent is justified for an aircraft, as the relative vertical load transfers occurring during braking stay limited.

E. Model Summary

The six control inputs of the model, the actuators states and the wind disturbance vector are represented, in Fig. 2, in light green, dark green and brown respectively. The standard aircraft states used to compute the ground effects are shown in blue, along with the six landing gear states, in Fig. 8, which summarizes the ground interaction model proposed. All relevant data regarding that module are reported in Table I and are relative to an Airbus A320 on a dry runway. Extra information concerning aerodynamic, propulsive and actuation modules can be found in [5].

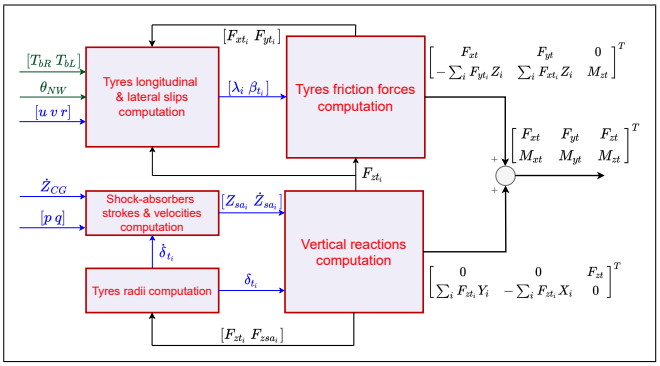

Fig. 8. Ground interaction model summary

TABLE I

RELEVANT NUMERICAL VALUES FOR AN AIRBUS A320[1] AND A DRY RUNWAY

Parameter	Unit	Value
m	kg	57×10^3
I_{xx} / I_{yy} / I_{zz}	$\mathrm{kg\cdot m^2}$	$(1.1\ /\ 2.9\ /\ 4.0)\ \times10^6$
I_{xy} / I_{yz} / I_{xz}	$\mathrm{kg\cdot m^2}$	$(0\ /\ 0\ /\ -1.4)\ \times10^5$
m_{NW} / m_{MG}	kg	120 / 910
$\mu_{s_{NW}}$ / $\mu_{s_{MG}}$	–	$(5\ /\ 3)\ \times10^{-4}$
$\mu_{b_{NW}}$ / $\mu_{b_{MG}}$	–	$(2\ /\ 1.5)\ \times10^{-4}$
$b_{sa_{NW}}$ / $b_{sa_{MG}}(compression)$	$\mathrm{N\cdot m^{-2}\cdot s^2}$	$(80\ /\ \{115;215\})\ \times10^3$
$b_{sa_{NW}}$ / $b_{sa_{MG}}(recoil)$	$\mathrm{N\cdot m^{-2}\cdot s^2}$	$(90\ /\ \{50;120\})\ \times10^3$
$B_{sa_{NW}}$ / $B_{sa_{MG}}(compression)$	$\mathrm{N\cdot m^{-\frac{2}{3}}\cdot s^{\frac{2}{3}}}$	$(39\ /\ \{54;101\})\ \times10^3$
$B_{sa_{NW}}$ / $B_{sa_{MG}}(recoil)$	$\mathrm{N\cdot m^{-\frac{2}{3}}\cdot s^{\frac{2}{3}}}$	$(44\ /\ \{24;57\})\ \times10^3$
$V_{tr_{NW}}$ / $V_{tr_{MG}}$	$\mathrm{m\cdot s^{-1}}$	0.58 / 0.57
k_{NW} / k_{MG}	$\mathrm{N\cdot m^{-1}}$	$(4.44\ /\ 3.37)\times10^6$
k_{NWt} / k_{MGt}	$\mathrm{N\cdot m^{-1}}$	$(2.75\ /\ 8.85)\times10^6$
λ_{opt} / μ_m / μ_l	–	0.09 / 0.6 / 0.24
σ / γ	–	0.09 / 2
X_{NW} / X_{MG}	m	11.14 / −1.7
Y_{NW} / $\lvert Y_{MG}\rvert$	m	0 / 3.795
$\lvert Y_{eng}\rvert$ / Z_{eng}	m	5.255 / 0.75
t_p	m	0.02
e_{NW} / e_{MG}	m	6.5×10^{-3} / 5×10^{-3}
c_1 / c_2 / c_3	–	0.1 / 0.9 / 0.2
k_1 / k_2	–	0.4 / 0.5
k_3 / k_4 / k_5	–	0.1 / 0.9 / 10
K_b	$\mathrm{N\cdot Pa^{-2}}$	5×10^{-3}

[1]Safran proprietary data have been deliberately distorted

III. MODEL VALIDATION

The validation of the proposed model is realized by comparison to a high fidelity multi-body simulator available at Safran Landing Systems. Different types of tests are performed, to separately check the vertical response alone, at first, and the coupled vertical-longitudinal dynamics secondly. The two scenarii hereafter reported and discussed are:

1) Scenario 1: drop test on single landing gear (allowing the study of F_{zt} only).

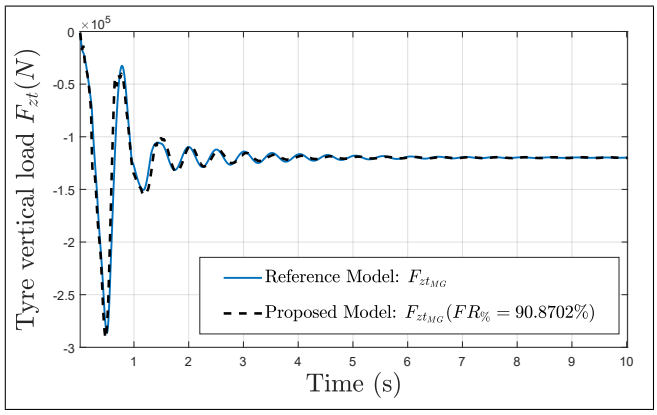

Fig. 9. Drop test: main gear tire vertical load

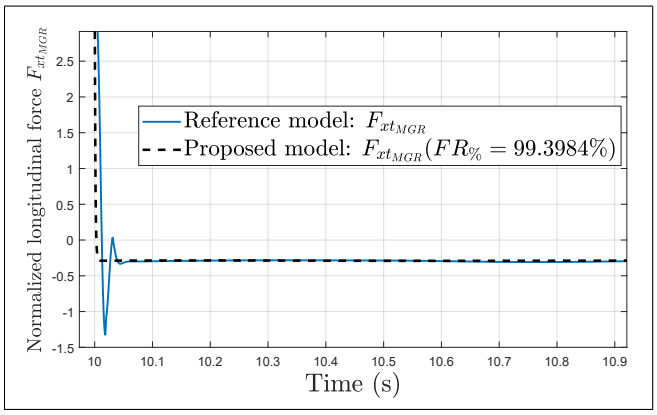

Fig. 11. Longitudinal braking: tire normalized longitudinal force (transient is magnified)

2) Scenario 2: longitudinal braking initiated at 10 s, on a dry runway, with a constant braking torque of $T_b = 2.1955\,10^4$ $N.m$.

Simulations are performed with the set of data reported in Table I, and completed by those in [5]. With the first scenario, the objective is to compare the vertical dynamic response by analyzing the F_{zt} time histories in terms of oscillations' amplitude, damping ratio, proper frequency and settling equilibrium values. The drop test, commonly used for landing gear testing, induces substantial reactions on the entire strut and shock-absorber, which undergoes the widest range of telescoping velocities tolerated. This allows to stress the system at its limits and validate its response at the edges of its operative domain. By the second scenario, the objective is to trigger vertical and longitudinal dynamic coupling through a hard brake during an aircraft roll-out phase. The same time-domain analysis is performed on F_{zt} and F_{xt} to evaluate the quality of the load transfer model together with the longitudinal friction one. The two scenarii together validate the overall 6-DOF aircraft on-ground model.

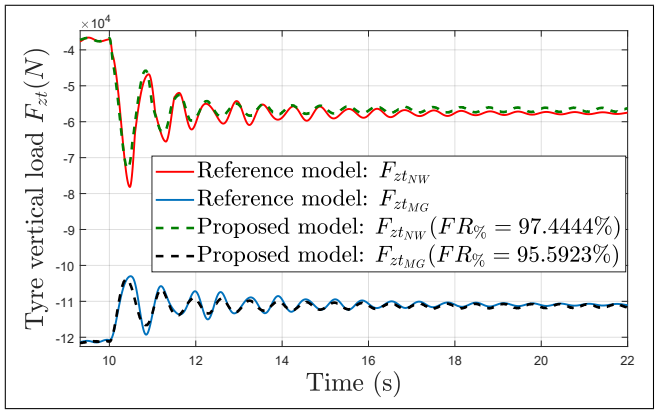

Fig. 10. Longitudinal braking: tire vertical loads

The obtained results are evaluated by means of a fitting ratio, between the reference model and the proposed model time histories, calculated over the relevant simulation time window as:

$$FR_{\%} = 100\left(1 - \frac{\int (y_{ref} - y_{model})^2\,dt}{\int (y_{ref})^2\,dt}\right) \tag{23}$$

where y_{ref} and y_{model} are the normalized signals. Commonly, a maximum 10% mismatch between obtained and reference dynamics has been observed in literature and industrial applications for similar case study, *i.e.* control oriented modeling ([5]), therefore it will be considered as the acceptance threshold for our model validation. As demonstrated by Figs. 9, 10 and 11, extremely satisfying fitting ratios are obtained in simulation *i.e.* 91% for the main landing gear during the drop test (97% for the nose landing gear not reported here); 95.6% and 97.4% respectively for main and nose landing gear during roll-out hard-braking mission. The high consistency in terms of amplitude, frequency and damping of the F_{zt} oscillatory response, observed in Figs. 9 and 10, can be read as the accuracy level of the shock-absorber and the load transfer modeling. Meanwhile, Fig. 11 shows the high precision of the implemented braking model, despite the different transient behavior justified by a simpler friction representation, as opposed to the reference dynamic friction model [29]. In addition, the simultaneous accuracy on F_{zt} and F_{xt} reached during braking demonstrates the ability to represent properly the variations of μ_x and of the corresponding wheel slip λ (see (15)), critical for control synthesis.

The degraded fitting ratios obtained for $F_{zt_{MG}}$ (Fig. 9 and 10) can be explained by the wider functioning domain of the system, due to larger equivalent mass supported. In addition, the proposed model appears to counteract recoiling motion at low stroke and high vertical velocity (first rebound peak) more strongly than the reference. This seems to be due to a small discrepancy between the two models' recoil damping coefficient values and variation law. However, frequency consistency still appears to be guaranteed, which is of paramount importance for the foreseen control oriented exploitation of the model. Room for slight improvement could be explored by choosing a smooth instead of an abrupt variation for the damping coefficients, especially $b_{sa_{MG}}$ (see Table I), and by incorporating a frequency dependency in the shock-

absorber spring hysteresis (f_{comp} and f_{rec}) to reduce the small oscillations' amplitude gap. This will obviously be at the expenses of a more complex model.

IV. CONCLUSION

A low complexity but accurate 6-DOF aircraft on-ground model intended for novel braking control law synthesis and suitable for fast simulation was proposed in this paper. Validation against a multi-body high-fidelity aircraft on-ground model available at Safran Landing Systems demonstrated the high level of representativeness reached. The original modeling choices made for capturing the critical vertical and longitudinal dynamic phenomena mostly concerned the shock-absorbers, the tire-ground friction representation and the wheel dynamics, as discussed throughout the paper. Their explicit, parametric formulations are easily adjustable to different landing-gear configurations and runway conditions, which is an extremely meaningful added value. The presented model will serve as benchmark for anti-skid controller design, implementation and validation, in the continuity of the same research project.

REFERENCES

[1] G. Van Es, "Running out of runway," Technical Report NLR-CR-2005-498 National Aerospace Laboratory NLR, 2005.

[2] ——, "A study of runway excursions from a European perspective," Technical Report NLR-TP-2010-259, 2010, Eurocontrol Report.

[3] "Safety report 2019, 56th edition," International Air Transport Association IATA, Tech. Rep., 2020, ISBN 978-92-9264-170-2. [Online]. Available: iata.org/publishing

[4] "Runway safety accident analysis report," International Air Transport Association IATA, Tech. Rep., 2015, ISBN 978-92-9252-776-1. [Online]. Available: iata.org/publishing

[5] E. Sadien, C. Roos, A. Birouche, M. Carton, C. Grimault, L. Romana, and M. Basset, "A simple and efficient control allocation scheme for on-ground aircraft runway centerline tracking," *Control Engineering Practice*, vol. 95, 2020.

[6] M. Cassaro and F. Courbun, "Method and device for assisting piloting of an aircraft moving on the ground," under patenting (EU-U.S.).

[7] F. Villaume, A. Jacob, and R. Lignee, "Method and device to assist in the piloting of an aircraft in a landing phase," U.S. Patent US8 209 072B2, 2008.

[8] Z. Ming, N. Hong, W. Xiao-hui, Q. Xiaomei, and Z. Enzhi, "Modeling and simulation of aircraft anti-skid braking and steering using co-simulation method," *COMPEL: The International Journal for Computation and Mathematics in Electrical and Electronic Engineering*, vol. 28, pp. 1471–1488, 2009.

[9] S. Gualdi, M. Morandini, and G. Ghiringhelli, "Anti-skid induced aircraft landing gear instability," *Aerospace Science and Technology*, vol. 12, pp. 627–637, 2008.

[10] E. B. Coetzee, B. Krauskopf, and M. Lowenberg, "Nonlinear aircraft ground dynamics," *International Conference on Nonlinear Problems in Aviation and Aerospace*, 2006.

[11] J. Biannic, A. Marcos, M. Jeanneau, and C. Roos, "Nonlinear simplified LFT modelling of an aircraft on ground," in *Proceedings of the IEEE Conference on Computer Aided Control System Design*, 2006, pp. 2213–2218.

[12] H. Georgieva and V. Serbezov, "Mathematical model of aircraft ground dynamics," in *Proceedings of the International Conference on Military Technologies*, 2017, pp. 514–519.

[13] W. R. Krüger and M. Morandini, "Numerical simulation of landing gear dynamics: state-of-the-art and recent developments," *Proceedings of Limit Cycle Oscillation and Other Amplitude-Limited Self Excited Vibrations, RTO-MP-AVT-152, Loen, Norway*, 2008.

[14] J. Duprez, F. Mora-Camino, and F. Villaume, "Control of the aircraft-on-ground lateral motion during low speed roll and manoeuvers," in *Proceedings of the IEEE Aerospace Conference*, 2004, pp. 2656–2666.

[15] E. Sadien, C. Roos, A. Birouche, C. Grimault, L. Romana, J. Boada-Bauxell, and M. Basset, "Control design oriented modeling of an on-ground aircraft," in *Proceedings of the European Control Conference*, 2018, pp. 2757–2762.

[16] A. G. Barnes and T. J. Yager, "Enhancement of aircraft ground handling simulation capability." AGARD-AG-333, 1998.

[17] P. H. Zipfel, *Modeling and Simulation of Aerospace Vehicle Dynamics, 2nd Ed.* AIAA (American Institute of Aeronautics & Astronautics), 2007.

[18] D. Feld, "An analytical investigation of damping of landing gear shimmy," in *SAE Technical Paper 902015*, 1990.

[19] S. Gan, X. Fang, and X. Wei, "Parametric analysis on landing gear strut friction of light aircraft for touchdown performance," *Applied Sciences*, vol. 11, no. 12, 2021.

[20] C. G. Scheck, "Thermal hysteresis loss in gas springs," Ph.D. dissertation, Ohio University, 1988.

[21] F. Löcken and M. Welsch, "The dynamic characteristic and hysteresis effect of an air spring," *International Journal of Applied Mechanics and Engineering*, vol. 20, pp. 127 – 145, 2015.

[22] A. Kornhauser and J. Smith, "The effects of heat transfer on gas spring performance," *Journal of Energy Resources Technology*, vol. 115, no. 1, pp. 70 – 75, 1993.

[23] J. C. Dixon, *The shock absorber handbook*. John Wiley & Sons, 2008.

[24] S. Andersson, A. Söderberg, and S. Björklund, "Friction models for sliding dry, boundary and mixed lubricated contacts," *Tribology International*, vol. 40, no. 4, pp. 580–587, 2007.

[25] F. Marques, P. Flores, J. Claro, and H. Lankarani, "Modeling and analysis of friction including rolling effects in multibody dynamics: a review," *Multibody System Dynamics*, vol. 45, 2019.

[26] ——, "A survey and comparison of several friction force models for dynamic analysis of multibody mechanical systems," *Nonlinear Dynamics*, vol. 86, pp. 1407–1443, 2016.

[27] S. M. Savaresi and M. Tanelli, *Active braking control systems design for vehicles*. Springer Science & Business Media, 2010.

[28] J. Svendenius and B. Wittenmark, "Review of wheel modeling and friction estimation," Department of Automatic Control, Lund Institute of Technology (LTH), Tech. Rep., 2003.

[29] C. C. de Wit, P. Tsiotras, E. Velenis, M. Basset, and G. Gissinger, "Dynamic friction models for road/tire longitudinal interaction," *Vehicle System Dynamics*, vol. 39, pp. 189–226, 03 2003.